A major purpose of the Technical Information Center is to provide the broadest dissemination possible of information contained in DOE's Research and Development Reports to business, industry, the academic community, and federal, state and local governments.

Although a small portion of this report is not reproducible, it is being made available to expedite the availability of information on the research discussed herein.

LA-UR -83-586

CONF-8209113--3

Los Alamos National Laboratory is operated by the University of California for the United States Department of Energy under contract W-7405-ENG-36.

LA-UR--83-506

DE83 009939

TITLE: CONVECTIVE TRANSPORT IN LASER TARGET PLASMAS

AUTHOR(S): J. U. Brackbill, Los Alamos National Laboratory
D. Colombant, Naval Research Laboratory, Washington, DC
N. Grandjouan, Ecole Polytechnique, Palaiseau, France

SUBMITTED TO: Proceedings of the 1982 CECAM Workshop on "The Flux Limiter and Heat Flow Instabilities", Orsay, France, September 13 - October 1, 1982.

DISCLAIMER

Los Alamos Los Alamos National Laboratory
Los Alamos, New Mexico 87545

FORM NO 836 R4
ST NO 2629 5/81

Convective Transport in Laser Target Plasmas

J. U. Brackbill
Los Alamos National Laboratory, Los Alamos, New Mexico, USA

D. Colombant
Naval Research Laboratory, Washington, DC, USA

and

N. Grandjouan
École Polytechnique, Palaiseau, France

Abstract

The role of guiding-center corrections in convective transport of electron energy is examined with a simple numerical model. At 10^{16} W cm^{-2} with a 60-μm spot and a 10.6-μm wavelength laser, the Righi-Leduc term is observed to have little effect on transport in a calculation with the thermal flux limited to the free-streaming value.

Introduction. Lateral transport of electron energy has been observed in laser target experiments with CO_2 lasers,[1,4] and recently with shorter wavelength lasers.[2] In these last experiments, as much as 30% of the absorbed laser energy is carried several millimeters from the laser spot.

Recent collisionless plasma-simulation results suggest that the lateral transport is due to self-generated magnetic fields.[3] In the simulations, a plasma is confined in a magnetic sheath that spreads across the target surface at speeds approaching 10^8 cm/s. Very strong collimation of the thermal flux beneath the laser spot into the target is observed, as well as inhibition of thermal diffusion by the sheath elsewhere. The trapping of the electron energy in the sheath results in a very large transfer of energy from the electrons to emitted fast ions. Many of these features have been observed in experiments. Especially striking are the bright regions corresponding to field nulls in multibeam experiments.[4]

A more complete theoretical understanding of lateral transport requires including collisions in the models. With collisions, physical length scales are introduced that will differentiate the results for various wavelength lasers. Of course, much fluid modeling has been done already.[5] For various reasons, lateral transport has not been observed to be a prominent feature of calculations with these models. One reason put forward is that the coronal plasma is insufficiently collisional to apply the usual transport theory.[6] Another, and the one explored here, is that competing convective terms in the fluid equations cancel the $\vec{E}\times\vec{B}$ drift motion of the electrons in the magnetic field.

To evaluate the relative importance of the various convection terms, a numerical approach is taken. For simplicity, the fluid equations with infinitely massive ions are examined. Furthermore, only the competition between the Righi-Leduc and $\vec{E}\times\vec{B}$ drift convective terms in the electron energy equation is considered. Within this restricted model, the scaling of these terms is examined, an explicit numerical algorithm to solve the fluid model equations is outlined, and numerical results are presented to illustrate the effect of magnetic field generation and the Righi-Leduc term on the lateral transport of electron energy.

A. The restricted fluid model.

In a model with infinitely massive ions and massless electrons, only Faraday's law and the electron energy equation are retained among the evolution equations. With standard notation[7] and in mks units, these equations may be written

$$\frac{\partial \vec{B}}{\partial t} = + \nabla\times\left(\vec{u}_e\times\vec{B}\right) - \nabla\times\left[\left(\nabla p_e + \vec{\beta}\cdot\nabla T_e\right)/ne\right] \tag{1}$$

and

$$\frac{1}{(\gamma-1)}\frac{\partial p_e}{\partial t} + p_e\left(\nabla\cdot\vec{u}_e\right) + T_e\nabla\cdot\vec{\beta}\cdot\vec{u}_e + \frac{1}{(\gamma-1)}\nabla\cdot p_e\vec{u}_e + \nabla\cdot\vec{Q}_e = P_{laser} . \tag{2}$$

In Faraday's law, Eq. (1), $\vec{B}$ is the magnetic field intensity, $\vec{u}_e$ is the electron drift velocity as given by Ampere's law,

$$\vec{u}_e = - \vec{J}/ne = - \nabla\times\vec{B}/\mu ne ,$$

$p_e = nkT_e$ is the electron pressure, n is the number density of electrons, e is the electron charge, and $\vec{\beta}$ is the thermoelectric coefficient. (Note that resistive diffusion is not included in the equation.) In the electron energy equation, $\vec{Q}_e$ is the heat flux, given by

$$\vec{Q}_e = - \vec{\kappa}\cdot\nabla T_e ,$$

where $\vec{\kappa}$ is the thermal conductivity tensor, and P_{laser} is a source term modeling the deposition of laser energy in the electrons.

For flow in a two-dimensional Cartesian geometry, Eqs. (1) and (2) can be further simplified. Where z is the ignored coordinate direction, the equations may be written in component form,

$$\frac{\partial B_z}{\partial t} = - \frac{\partial}{\partial x} u_x B_z - \frac{\partial}{\partial y} u_y B_z + \frac{\partial}{\partial x}\left[\left(\frac{\partial p}{\partial y} + \beta_\perp \frac{\partial T}{\partial y} + \beta_\wedge \frac{\partial T}{\partial x}\right)/ne\right]$$

$$- \frac{\partial}{\partial y}\left[\left(\frac{\partial p}{\partial x} + \beta_\perp \frac{\partial T}{\partial x} - \beta_\wedge \frac{\partial T}{\partial y}\right)/ne\right]$$

and

$$\frac{1}{(\gamma-1)}\frac{\partial p_e}{\partial t} + p_e\left(\frac{\partial u_{ex}}{\partial x} + \frac{\partial u_{ey}}{\partial y}\right) + T_e\left[\frac{\partial}{\partial x}\left(\beta_\perp u_{ex} + \beta_\wedge u_{ey}\right) + \frac{\partial}{\partial y}\left(\beta_\perp u_{ey} - \beta_\wedge u_{ex}\right)\right]$$

$$+ \frac{1}{(\gamma-1)}\left(\frac{\partial}{\partial x}\, p_e u_{ex} + \frac{\partial}{\partial y}\, p_e u_{ey}\right) = \frac{\partial}{\partial x}\left(\kappa_\perp\frac{\partial T}{\partial x} + \kappa_\wedge\frac{\partial T}{\partial y}\right) + \frac{\partial}{\partial y}\left(\kappa_\perp\frac{\partial T}{\partial y} - \kappa_\wedge\frac{\partial T}{\partial x}\right),$$

where $\beta_\perp$ and $\beta_\wedge$ correspond to $\beta_\perp^{Tu}$ and $\beta_\wedge^{Tu}$ in Braginskii.

B. The convection terms.

Among the various terms in the fluid model, three convection terms can be identified. The first, the electron drift velocity, $\vec{u}_e$, corresponds to the velocity of the frame in which the electric field due to finite electron pressure, $\vec{E} = -\nabla p_e/ne$, is zero in steady state. As described elsewhere,[3] the drift velocity scales relative to the electron thermal speed as the ratio of the collisionless skin depth, c/ω_{pe}, to the density gradient scale length, L_n,

$$\left|\vec{u}_e\right| \approx cv_{th}/\omega_{pe}L_n \ .$$

Less explicit in Eqs. (1) and (2) is the convection due to guiding center correction terms.

The thermoelectric term in Faraday's law and the heat flux terms in the electron energy equation contain terms in which the highest derivative of the dependent variable is the first derivative. These are convective rather than diffusive. For example, among the thermoelectric terms is the Nernst term, which can be written,

$$\nabla\times\beta_\wedge(\hat{b}\times\nabla T_e) = +\nabla\times(\vec{u}_N\times\vec{B}) \ ,$$

where

$$\hat{b} \equiv \vec{B}/\left|\vec{B}\right|$$

and

$$\vec{u}_N \equiv -\beta_\wedge\nabla T_e/\left|\vec{B}\right| \ .$$

The effect of this term has been investigated earlier by Colombant and Winsor.[5] Scaling estimates indicate that $\vec{u}_N$ is largest when there is no field to convect.[6] The term will not be considered further here.

The convective term in the heat flux can be written

$$\nabla\cdot\kappa_{\wedge}(\hat{b}\times\nabla T_e) = \vec{u}_R\cdot\nabla T_e \ ,$$

where the Righi-Leduc velocity is defined by

$$\vec{u}_R \equiv \nabla\times\kappa_{\wedge}\hat{b} \ . \tag{3}$$

Following Braginskii, $\kappa_{\wedge}$ is written

$$\kappa_{\wedge} = \frac{nT_e\tau_e}{m_e}\,\frac{\chi\left(\gamma_1''\chi^2 + \gamma_0''\right)}{\Delta} \ ,$$

where τ_e is the mean free time between collisions, $\chi \equiv \omega_{ce}\tau_e$, ω_{ce} is the electron cyclotron frequency, and

$$\Delta \equiv \chi^4 + \delta_1\chi^2 + \delta_0 \ .$$

(The constants, γ_1'', γ_0'', δ_1 and δ_0 are all O(1).)

For an unmagnetized plasma, $\kappa_{\wedge}$ is zero reflecting its origin in finite electron gyroradius effects. In a weakly collisional plasma with $v_{th}\tau_e/L_T \gg 1$, χ may be O(1) even though $\omega_{ce} \ll 1$ so that $\vec{u}_R$ is very large. Of course, the coefficients are not valid in this limit. Nevertheless, this is an extreme case where the convection due to the Righi-Leduc term is larger than the convection due to drift. It is to examine the competition between the Righi-Leduc and drift terms in less extreme cases that numerical solutions are now sought.

C. The numerical algorithm.

The electron transport equations are approximated by finite difference equations on a uniform rectilinear mesh with constant interval Δx in x and Δy in y. The dependent variables, $\vec{B}$, $\vec{u}_e$, p_e and T_e, are stored at the centers of cells. Spatial derivatives in the transport equations are approximated by centered differences on the mesh.

The solution evolves as the finite difference equations are marched with time step Δt. Derivatives with respect to time are explicit; all quantities appearing on the right-hand side of the difference equations are available at the beginning of the time step.

The difference equations are listed with a simplified notation. All quantities available at the beginning of the n^{th} time step are unlabeled as to time. Where the indices of each cell are (i,j), the dependent variables are labeled ϕ_i^j. Furthermore, the subscript e is dropped since there is only one fluid, $\vec{B}$ is simply $\hat{z}B$ since there is only one field component and $\vec{u}_e$ is replaced by (u,v). The finite difference equations are now given.

The components of the electron drift velocity are given by

$$u_i^j = -\left(B_i^{j+1} - B_i^{j-1}\right)/2\mu_0 n_i^j e\Delta y$$

and

$$v_i^j = \left(B_{i+1}^j - B_{i-1}^j\right)/2\mu_0 n_i^j e\Delta x \quad ,$$

where μ_0 is the permeability.

Faraday's law is approximated by

$$\begin{aligned}\left(B_i^j\right)^{n+1} = B_i^j + \Big\{ &- \left(u_{i+\frac{1}{2}}^j B_{i+\frac{1}{2}}^j - u_{i-\frac{1}{2}}^j B_{i-\frac{1}{2}}^j\right)/\Delta x - \left(v_i^{j+\frac{1}{2}} B_i^{j+\frac{1}{2}} - v_i^{j-\frac{1}{2}} B_i^{j-\frac{1}{2}}\right)/\Delta y \\ &+ \left[\left(P_{i+1}^{j+1} - P_{i+1}^{j-1}\right)/2n_{i+1}^j e\Delta y - \left(P_{i-1}^{j+1} - P_{i-1}^{j-1}\right)/2n_{i-1}^j e\Delta y\right]/2\Delta x \\ &- \left[\left(P_{i+1}^{j+1} - P_{i-1}^{j+1}\right)/2n_i^{j+1} e\Delta x - \left(P_{i+1}^{j-1} - P_{i-1}^{j-1}\right)/2n_i^{j-1} e\Delta x\right]/2\Delta y \\ &+ \Big[\beta_{\perp i+\frac{1}{2}}^j\left(T_{i+1}^{j+1} - T_{i+1}^{j-1}\right) - \beta_{\perp i-\frac{1}{2}}^j\left(T_{i-1}^{j+1} - T_{i-1}^{j-1}\right) \\ &\qquad - \beta_{\perp i}^{j+\frac{1}{2}}\left(T_{i+1}^{j+1} - T_{i-1}^{j+1}\right) + \beta_{\perp i}^{j-\frac{1}{2}}\left(T_{i+1}^{j-1} - T_{i-1}^{j-1}\right)\Big]/2\Delta x\Delta y \\ &+ \left[\beta_{\wedge i+\frac{1}{2}}^j\left(T_{i+1}^j - T_i^j\right) - \beta_{\wedge i-\frac{1}{2}}^j\left(T_i^j - T_{i-1}^j\right)\right]/\Delta x^2 \\ &- \left[\beta_{\wedge i}^{j+\frac{1}{2}}\left(T_i^{j+1} - T_i^j\right) - \beta_{\wedge i}^{j-\frac{1}{2}}\left(T_i^j - T_i^{j-1}\right)\right]/\Delta y^2\Big\}\Delta t \ .\end{aligned}$$

All of the terms labelled by half-integer indices are defined by linear averages except B. For example, $u^j_{i+\frac{1}{2}}$ is given by

$$u^j_{i+\frac{1}{2}} = \frac{1}{2}\left(u^j_{i+1} + u^j_i\right) .$$

The terms containing half-integer values of B are defined differently to give stability to terms containing convective derivatives. The face-centered values of B are defined by linear interpolation,

$$B^j_{i+\frac{1}{2}} = \frac{1}{2}\left[\left(1 - \alpha^j_{i+\frac{1}{2}}\right)B^j_{i+1} + \left(1 + \alpha^j_{i+\frac{1}{2}}\right)B^j_i\right] ,$$

and

$$B^{j+\frac{1}{2}}_i = \frac{1}{2}\left[\left(1 - \alpha^{j+\frac{1}{2}}_i\right)B^{j+1}_i + \left(1 + \alpha^{j+\frac{1}{2}}_i\right)B^j_i\right] ,$$

where α, the interpolation coefficient, depends on the velocity, $\vec{u}_e$, and its gradients. Briefly, as in similar algorithms developed by Zalesak,[9] α changes in value from $u\Delta t/\Delta x$ as in interpolated donor cell[10] to either 1 or -1 as the length scale of variation of the velocity approaches the mesh spacing. The interpolation parameter α is given by

$$\alpha^j_{i+\frac{1}{2}} = \left(1 - \Delta^j_{i+\frac{1}{2}}\right)u^j_{i+\frac{1}{2}}\Delta t/\Delta x + \Delta^j_{i+\frac{1}{2}}\,\mathrm{sign}\left(1, u^j_{i+\frac{1}{2}}\right) ,$$

and

$$\alpha^{j+\frac{1}{2}}_i = \left(1 - \Delta^{j+\frac{1}{2}}_i\right)v^{j+\frac{1}{2}}_i\Delta t/\Delta x + \Delta^{j+\frac{1}{2}}_i\,\mathrm{sign}\left(1, v^{j+\frac{1}{2}}_i\right) ,$$

where Δ, the switching parameter, is defined by

$$\Delta^j_i = \min\left(1, \delta^j_i\right) ,$$

and δ^j_i, the measure of the velocity gradient scale length is defined by

$$\delta^j_i = \left\{\left[\left(u^j_{i+1} - u^j_{i-1}\right)/u^j_i\right]^2 + \left[\left(v^{j+1}_i - v^{j-1}_i\right)/v^j_i\right]^2\right\}^{1/2} .$$

Using these equations for the convection terms results in stability when $u\Delta t/\Delta x < 1$, and positive diffusivity for arbitrary gradients in $\vec{u}_e$.

The electron energy equation is differenced similarly,

$$\left(P_i^j\right)^{n+1} = P_i^j + (\gamma-1)\Bigg\{ - P_i^j\left[\left(\tilde{u}_{i+1}^j - \tilde{u}_{i-1}^j\right)/2\Delta x + \left(\tilde{v}_i^{j+1} - \tilde{v}_i^{j-1}\right)/2\Delta y\right]$$

$$- T_i\left[\left(\beta_{\perp i+1}^j \tilde{u}_{i+1}^j + \beta_{\wedge i+1}^j \tilde{v}_{i+1}^j - \beta_{\perp i-1}^j \tilde{u}_{i-1}^j - \beta_{\wedge i-1}^j \tilde{v}_{i-1}^j\right)/2\Delta x\right.$$

$$\left. + \left(\beta_{\perp i}^{j+1}\tilde{v}_i^{j+1} - \beta_{\wedge i}^{j+1}\tilde{u}_i^{j+1} - \beta_{\perp i}^{j-1}\tilde{v}_i^{j-1} + \beta_{\wedge i}^{j-1}\tilde{u}_i^{j-1}\right)/2\Delta y\right]$$

$$- \left(\tilde{u}_{i+\frac{1}{2}}^j P_{i+\frac{1}{2}}^j - \tilde{u}_{i-\frac{1}{2}}^j P_{i-\frac{1}{2}}^j\right)/(\gamma-1)\Delta x + \left(\tilde{v}_i^{j+\frac{1}{2}} P_i^{j+\frac{1}{2}} - \tilde{v}_i^{j-\frac{1}{2}} P_i^{j-\frac{1}{2}}\right)/(\gamma-1)\Delta y$$

$$+ \left[\kappa_{\perp i+\frac{1}{2}}^j\left(T_{i+1}^j - T_i^j\right) - \kappa_{\perp i-\frac{1}{2}}^j\left(T_i^j - T_{i-1}^j\right)\right]/\Delta x^2$$

$$- \left[\kappa_{\wedge i+1}^j\left(T_{i+1}^{j+1} - T_{i+1}^{j-1}\right) - \kappa_{\wedge i-1}^j\left(T_{i-1}^{j+1} - T_{i-1}^{j-1}\right)\right]/4\Delta x\Delta y$$

$$+ \left[\kappa_{\wedge i}^{j+1}\left(T_{i+1}^{j+1} - T_{i-1}^{j+1}\right) - \kappa_{\wedge i}^{j-1}\left(T_{i+1}^{j-1} - T_{i-1}^{j-1}\right)\right]/4\Delta x\Delta y$$

$$+ \left[\kappa_{\perp i}^{j+\frac{1}{2}}\left(T_i^{j+1} - T_i^j\right) - \kappa_{\perp i}^{j-\frac{1}{2}}\left(T_i^j - T_i^{j-1}\right)\right]/\Delta y^2 + P_{laser}\Bigg\}\,\Delta t\,.$$

The values of P at half-integer positions are calculated as are corresponding values of B,

$$P_{i+\frac{1}{2}}^j = \frac{1}{2}\left[\left(1 - \alpha_{i+\frac{1}{2}}^j\right)P_{i+1}^j + \left(1 + \alpha_{i+\frac{1}{2}}^j\right)P_i^j\right]$$

and

$$P_i^{j+\frac{1}{2}} = \frac{1}{2}\left[\left(1 - \alpha_i^{j+\frac{1}{2}}\right)P_i^{j+1} + \left(1 + \alpha_i^{j+\frac{1}{2}}\right)P_i^j\right]\,.$$

To be consistent, the Righi-Leduc terms ought also to be treated as convection terms. However, if their contribution is sufficiently small they should have little impact on the overall stability.

The barred velocities, $\tilde{u}_i^j$ and $\tilde{v}_i^j$, represent averages between values of $\vec{u}_e$ at t and t+Δt. These values, which are time-centered, are used so that energy is conserved. Their evaluation requires that $\vec{u}_e$ be calculated after advancing B_i^j as well as before.

The time step for the calculation is variable. It is chosen to satisfy the Courant limit corresponding to the thermal magnetic wave discussed by Pert,[5]

$$\left(v_{th}^2 + c^2/\omega_{pe}^2 L_n^2\right)\Delta t^2 < 1/\left(1/\Delta x^2 + 1/\Delta y^2\right) ,$$

and the explicit diffusion-limited time step,

$$\underset{i,j}{\text{Max}}\left(H_{\perp_1}^j\right)\Delta t < \frac{1}{2}\left[1/\left(1/\Delta x^2 + 1/\Delta y^2\right)\right] .$$

These conditions are calculated at the beginning of the time step. So that they are sufficient after laser energy has been deposited, the time step is also limited to restrict the maximum relative change in the energy.

D. Numerical Results.

When a slab of plasma is illuminated by an intense, focussed laser beam, electron transport should occur by both diffusive and convective processes. The large temperature gradients drive the thermal diffusion term, and the temperature and density gradients acting together generate a magnetic field.

Here the separate effect of diffusion- and magnetic-field-enhanced convective transport are examined numerically. With the simple model outlined previously, transport is calculated with and without self-generated fields, with and without a flux limiter, and with and without the guiding center corrections to the thermal diffusion term.

As in the calculations with VENUS, the case of a slab of plasma in Cartesian geometry is considered.[3,8] A laser beam propagating in the negative x-direction (vertical axis) deposits energy along an infinite line in z with full width at half maximum equal to 60 μm. The target, whose number density increases linearly from a background value of 1.5×10^{23} m^{-3} to a maximum value of 1.5×10^{25} m^{-3} over a distance in x of 15 μm, is at an initial temperature of ≈ 1 eV. The laser intensity rises from zero to a maximum value of 10^{16} W/cm^2 in 10 ps. The intensity is maximum at the center of the line with a Gaussian variation in y.

The numerical computations are performed on a 20x20 zone mesh with $\Delta x = 5$ μm and $\Delta y = 15$ μm. Where x_{crit} is the x-position of the critical density surfce, 80% of the laser energy is deposited in the neighboring cell with $x < x_{crit}$ and $\rho \geq \rho_{crit}$, and 20% in the neighboring cell with $x > x_{crit}$ and $\rho < \rho_{crit}$.

The right boundary of the mesh is a plane of symmetry where $\partial T/\partial y = 0$ and $B = 0$. Only the left half of the target is modelled. On the bottom, top and left boundaries, $T = T_{background}$ exterior to the mesh. All other dependent variables have zero normal derivative.

A comparison of the results of calculations for the cases listed above is shown in Fig. 1 at $t = 10$ ps. When Faraday's law is not advanced so that $B \equiv 0$ (the unmagnetized case), the results shown in Figs. 1a and 1b are obtained. The temperature contours in Fig. 1a show that diffusion has carried electron energy further from the source in the low-density plasma. However, the thermal flux vectors ($-\kappa_\perp \nabla T$) in Fig. 1a show that more energy is carried into the high-density plasma beneath the spot than into the low-density plasma above, evidently because of the lower temperature gradients in the low-density plasma.

In Fig. 1b, a similar calculation is depicted with the thermal flux limited to the classical, free-streaming value. The limiter compares the mean free path, $v_{th}\tau_e$, with the thermal gradient length, and limits the flux where this ratio exceeds one by replacing κ by κ', where κ' is defined by

$$\kappa'_{\perp,\wedge} \equiv \kappa_{\perp,\wedge}/(1 + v_{th}\tau_e/L_T) \ ,$$

and L_T is the thermal gradient scale length. As shown by the temperature contours in Fig. 1b, the limiter traps energy in the source region and increases the maximum temperature from 3.4×10^6 K (without a limiter) to 5.3×10^6 K. Paradoxically, the limiter also increases the maximum thermal flux.

The limiter steepens gradients where the plasma is least collisional, even though collisionless plasma simulations suggest that a lack of collisionality should smooth gradients.[3] That is, in the collisionless limit, the flux-limited fluid equations and the collisionless plasma simulations disagree.

With the magnetic field on, the results are as shown in Figs. 1c and 1d. Without a flux limit, the electron temperature contours shown in Fig. 1c are similar to those for the unmagnetized case except for the strong temperature gradient in the source region and behind it. However, as a result of these differences, the thermal flux into the overdense plasma is twice as large in the magnetized case, and the thermal flux into the underdense plasma is invisible in the plot.

With a flux limiter on, the corresponding electron temperature contours shown in Fig. 1d are very different from either the unmagnetized case without a flux limiter, Fig. 1a, or the magnetized case without a flux limiter, Fig. 1c. The maximum temperature is ten times as high and is localized at the edge of the laser spot. The thermal flux shown in Fig. 1d is even more strongly collimated into the overdense material.

In Fig. 2, the Righi-Leduc velocity defined by Eq. (3) is plotted. When there is no flux limiter, the maximum Righi-Leduc velocity (Fig. 2a) is 100 c. The velocity is so large that the corresponding terms in the electron energy equation must be nulled if one is to do a calculation in a reasonable amount of computing time because of the stability limit on the time step. When there is a flux limiter, the maximum Righi-Leduc velocity is 0.5 c. The velocity is still large, but including or not including the corresponding terms in the electron energy equation has little apparent effect on the solution, thus answering one of the questions posed by this study. (The results shown in Fig. 3 at a later time include the contribution from the Righi-Leduc term.)

At 50 ps, the magnetic sheath described earlier is fully formed as shown in Fig. 3. Figures 3a, b, c, d and e depict the electron drift velocity, the magnetic field, the electron temperature, $\omega_{ce}\tau_e$, and the thermal flux, $\kappa_\perp \nabla T$, respectively. (The electron temperature plot is mislabelled; the units are K.)

On the left, the results with a flux limiter are shown; on the right, those without. In both examples, lateral drift is associated with confinement of the electrons in a magnetized sheath, high values of $\omega_{ce}\tau_e$, and restriction of thermal flux into the dense material below to the region behind the spot. Differences result from applying the limiter, which tends to raise the electron temperature. At higher temperatures, the magnetic

field spreads more rapidly and is stronger. (It is so strong, in fact, that the electron drift speed exceeds c.)

E. Discussion.

The numerical model is simple, yet capable of answering questions unanswerable by analysis. For example, the computations demonstrate that the Righi-Leduc guiding center correction term does not suppress magnetically enhanced lateral transport. However, the numerical calculation answers the question only for the case calculated and thus only suggests that other problems might give similar results.

An unanswered question is raised by the dependence of the results on the flux limiter. The question is not so much the exact form of the limiter, or even what fraction of the classical free-streaming value the thermal flux is allowed to reach. Rather, it is whether a flux limiter is the appropriate way to impose reasonable behavior on fluid equations in the collisionless limit. It has been argued that the diffusion equations with a flux limiter give the correct integrated flux. However, it is clear from the model equations and numerical results that the magnetic field generation depends on temperatures and temperature gradients, both of which are dependent on the limiter.

REFERENCES

1. N. A. Ebrahim, C. Joshi, D. M. Villeneuve, N. H. Burnett, and M. C. Richardson, Phys. Rev. Lett. 43 (1979) 1995; P. A. Jaanimagi, N. A. Ebrahim, N. H. Burnett, and C. Joshi, Appl. Phys. Lett. 42 (1979) 1216; R. Decoste, J. C. Kieffer, and H. Pépin, Phys. Rev. Lett. 47 (1981) 35.

2. F. Amiranoff, K. Eidmann, R. Sigel, R. Fedosejevs, A. Maaswinkel, and Yung-lu Teng, J. D. Kilkenny, J. D. Hares, D. K. Bradley, B. J. MacGowan, and T. J. Goldsack, J. Phys. D: Appl. Phys. 15 (1982) 2463; T. J. Goldsack, J. D. Kilkenny, B. J. MacGowan, P. F. Cunningham, C. L. S. Lewis, M. H. Key, and D. T. Rumsby, Phys. Fluids 25 (1982) 1634.

3. D. W. Forslund and J. U. Brackbill, Phys. Rev. Lett. 48 (1982) 1614.

4. M. A. Yates et al., Phys. Rev. Lett. 49 (1982) 1702.

5. J. B. Chase, J. M. LeBlanc, and J. R. Wilson, Phys. Fluids 16 (1973) 1142; D. G. Colombant, K. , Whitney, D. A. Tidman, N. K. Winsor, and J. Davis, Phys. Fluids 18 (1976) 1687; D. G. Colombant and N. K. Winsor, Phys. Rev. Lett. 38 (1977) 697; R. S. Craxton and M. G. Haines, Plasma Physics 20 (1978) 487; J. D. Christiansen and N. K. Winsor, J. Comput. Phys. 35 (1980) 291; P. D. Nielson and G. B. Zimmerman, UCRL-53123, February 1981; C. J. Pert, J. Comput. Phys. 43 (1981) 111.

6. J. U. Brackbill and S. R. Goldman, submitted Comm. Pure Appl. Math.

7. S. I. Braginskii, Reviews of Plasma Physics 1 (1965) 205.

8. J. U. Brackbill and D. W. Forslund, J. Comput. Phys 46 (1982) 271.

9. S. T. Zalesak, J. Comp. Phys. 31 (1979) 335.

10. R. A. Gentry, R. E. Martin and B. J. Daly, J. Comp. Phys. 46 (1982) 342.

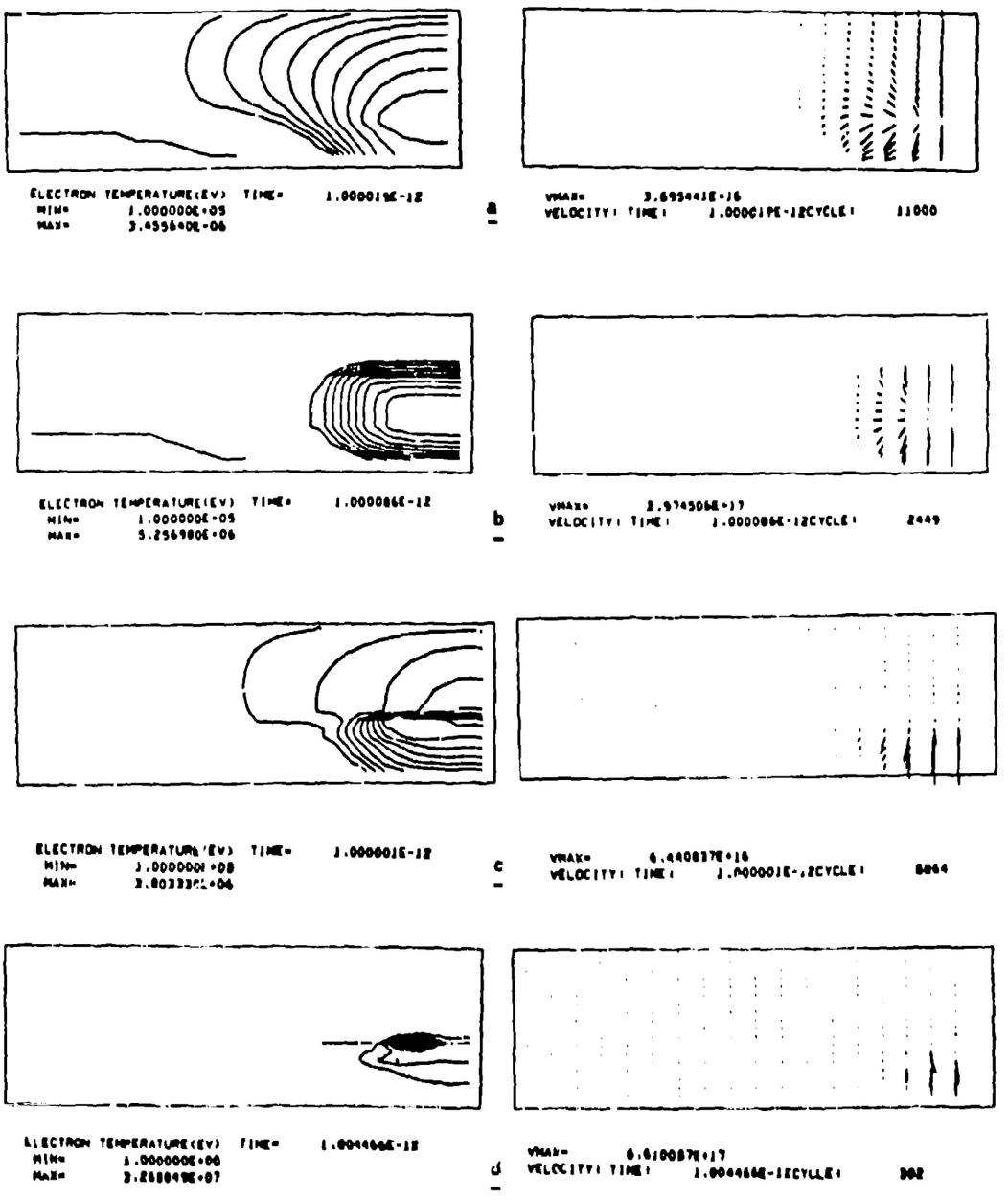

Fig. 1. A comparison of temperature distributions and thermal fluxes for various calculations is shown. The calculations are: unmagnetized without flux limiting (1a), unmagnetized with flux limiting (1b), magnetized without flux limiting (1c) and magnetized with flux limiting (1d).

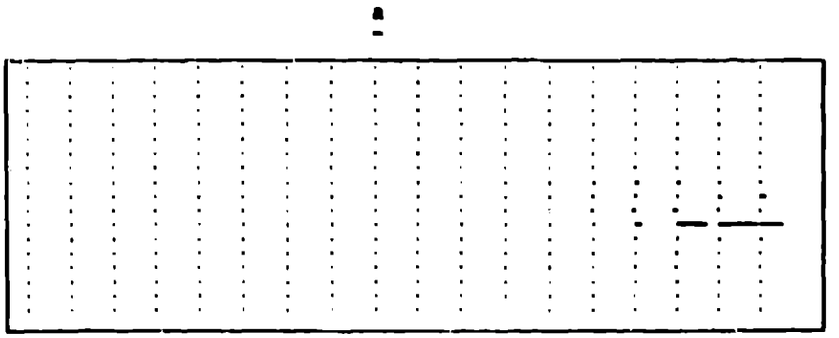

VMAX= 2.540962E+10
VELOCITY: TIME: 1.000001E-12CYCLE: 5864

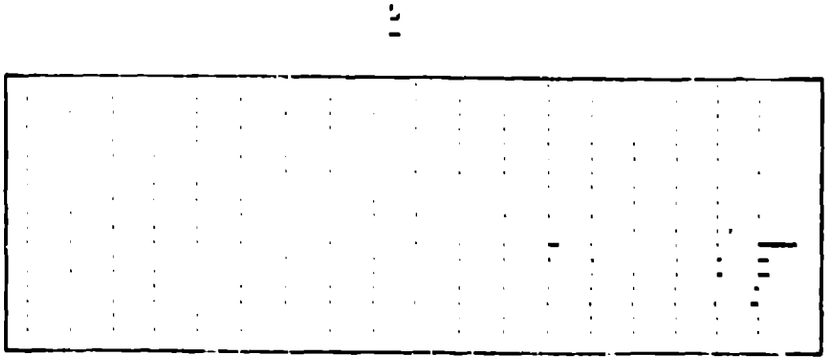

VMAX= 1.442898E+08
VELOCITY: TIME: 1.000492E-12CYCLE: 140

Fig. 2. The Right-Leduc velocity without flux limiting (2n) exceeds the speed of light. With flux limiting, the velocity is smaller and has little effect on transport.

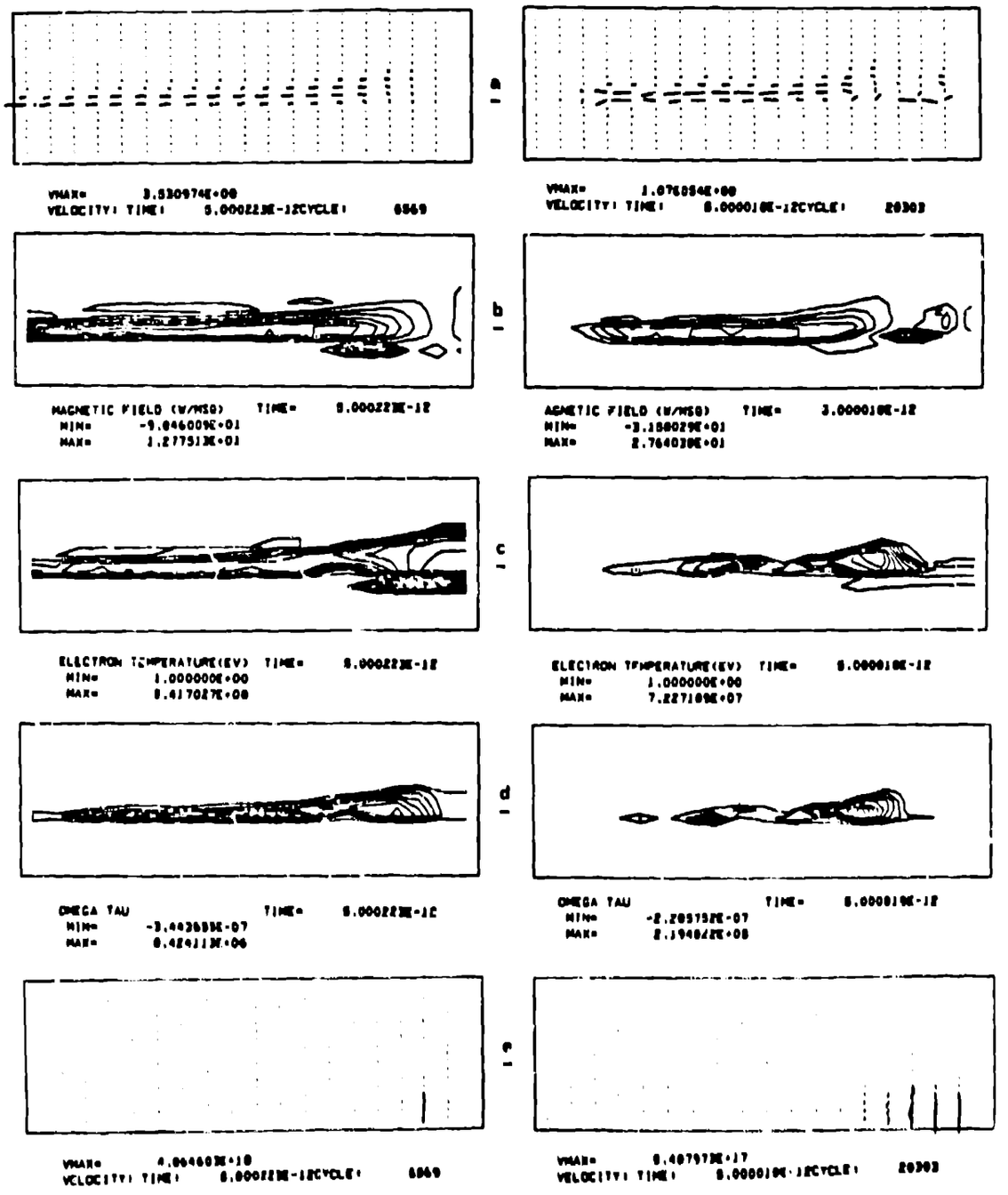

Fig. 3. A comparison of the magnetized case with flux limiting on the left, and without flux limiting on the right, is shown at 50 ps. Without flux limiting, more transport into the dense material occurs, the maximum temperature is lower and the thermal-magnetic wave speed is slower. Nevertheless, $\omega_{ce}\tau_e$ is very large.